Dynamic Causal Modeling of load-dependent modulation of effective connectivity within the verbal working memory network

Short title: Brain connectivity in increasing memory load

Danai Dima[1], Jigar Jogia[1], Sophia Frangou[2]

[1] Institute of Psychiatry, King's College London, London, UK

[2] Icahn School of Medicine at Mount Sinai, New York, USA

Keywords: neuroimaging; fMRI; N-back task; dorsolateral prefrontal cortex; **short-term plasticity**; parietal; anterior cingulate

Abstract

Neuroimaging studies have consistently shown that working memory (WM) tasks engage a distributed neural network that primarily includes the dorsolateral prefrontal (DLPFC), the parietal (PAR) and the anterior cingulate cortices (ACC). The current challenge is to provide a mechanistic account of the changes observed in regional activity. To achieve this we characterised neuroplastic responses in effective connectivity between these regions at increasing WM loads using Dynamic Causal Modeling of functional magnetic resonance imaging data obtained from healthy individuals during a verbal n–back task. Our data demonstrate that increasing memory load was associated with (a) right-hemisphere dominance, (b) increasing forward (i.e. posterior to anterior) effective connectivity within the WM network, and (c) reduction in individual variability in WM network architecture resulting in the right-hemisphere forward model reaching an exceedance probability of 99% in the most demanding condition. Our results provide direct empirical support that task difficulty, in our case WM load, is a significant moderator of **short-term plasticity**, complementing existing theories of task-related reduction in variability in neural networks.

Introduction

Working memory (WM) refers to the ability to maintain, update and manipulate goal-relevant information (Baddeley, 1992). WM tasks consistently recruit cortical regions within the dorsolateral prefrontal cortex (DLPFC, Brodmann Area 9/46), the parietal cortex (PAR, BA7/40) and the dorsal anterior cingulate cortex (ACC, BA32) (Fletcher and Henson, 2001; Wager and Smith, 2003; Nee et al., 2013). Within this network, there is evidence for relative functional specialisation according to process; the DLPFC has been intimately linked to encoding, setting attentional priorities and manipulating information (D' Esposito et al., 2000; Narayanan et al., 2005), the PAR has been associated with maintaining attentional focus and storing information (Jonides et al., 1998; Guerin and Miller, 2011) and the ACC has been implicated in error detection and performance adjustment (Carter et al., 1999). Regional activation within this network responds to WM load (i.e. the total demand on maintenance, updating and manipulation processes) (Braver et al., 1997; Callicott et al., 1999; Owen et al., 1999; Volle et al., 2008) and may be sensitive to content being left-lateralised for verbal and right-lateralised for spatial and object information (Fletcher and Henson, 2001; Wager and Smith, 2003; Nee et al., 2013).

However, measures of regional engagement are not sufficient to characterise the dynamic architecture of the WM network. To date, attempts to model inter-regional relationships within the WM network have been based **on minimizing the discrepancy between observed and implied correlations between regional activations** (Honey et al., 2002; Narayanan et al., 2005; Axmacher et al., 2008; Esslinger et al., 2012). Although useful, this approach provides limited information about specific mechanisms through which **neuronal circuits** respond to WM demands **(Ramnani et al., 2004; Kim et al., 2007)**. Of particular relevance is the potential role of **short-term plasticity** given the confluence of

evidence that abnormalities in **short-term plasticity** underlie WM impairment across a range of conditions from normal aging (Sala-Llonch et al., 2012) to the major mental disorders (Cramer et al., 2011). **Short-term plasticity** is conceptualized in many ways, but as used here it refers to altered functional coupling within cortical circuits as a function of experience **and in response to external and internal cues (Salinas & Sejnowski, 2001**; Stephan et al., 2009). Dynamic Causal Modeling (DCM; Friston et al., 2003) currently represents one of the most plausible methods for estimating the effective strength of connections among neuronal ensembles and their context-dependent (e.g. experimental) modulation (Stephan et al., 2010).

The aim of the current study was to probe the neural network that underlies **cognitive control in** verbal WM and to determine the role of WM load on **short-term plasticity** within this network. To achieve this we combined Statistical Parametric Mapping (SPM; www.fil.ion.ucl.ac.uk/spm) with Dynamic Causal Modeling of functional magnetic resonance imaging (fMRI) data derived from forty healthy adults performing the verbal n-back task. This task involves maintenance and updating of information at increasing levels of memory load and has been previously shown to engage robustly the DLPFC, PAR and ACC (Wager and Smith, 2003; Owen et al., 2005). DCM analysis of individual responses to this task allowed us to estimate the strength, laterality and directionality of the effective functional coupling between these key nodes of the WM network and, crucially how these connection strengths were modulated by memory load.

Material and Methods

Participants

Forty healthy right-handed adults were recruited via advertisement in the local press and were included if they (i) had no personal lifetime history of mental disorders or substance use as assessed following personal interview using the Structured Interview for DSM-IV-TR Axis I Disorders, non-patient edition (First et al., 2002), (ii) had no history of head injury or medical disorders and (iii) did not take any prescribed medication. An estimate of current intellectual function (IQ) was obtained using the Wechsler Adult Intelligence Scale – Revised (WAIS-R; Wechsler, 1981). The sample details are shown in Table 1. The study was approved by the Ethics Committee of the Institute of Psychiatry and the South London and Maudsley National Health Service Trust. Written informed consent was obtained from all participants.

Experimental design

The n-back task was employed in a block design incorporating alternating experimental and baseline conditions. A series of letters in yellow font were displayed on a blue screen for two seconds each. The 0-back condition was used as baseline to control for task engagement and vigilance. In the 0-back condition participants were instructed to respond by button press whenever the target letter "X" was displayed on screen. In the experimental conditions (1, 2, 3-back), the target letter was defined as any letter that was identical to the one presented 1, 2, or 3 trials back. There were 18 epochs in all, each lasting 30 seconds, comprising 14 letters with a ratio of target to non-target letters ranging from 2:12 to 4:10 per epoch. The entire experiment lasted 9 minutes and included a total of 49 target and 203 non-target stimuli. To avoid any systematic order effects the conditions were

pseudo-randomised. Performance was evaluated in terms of reaction time to target letters and accuracy (% correct responses).

Image acquisition

Gradient echo planar magnetic resonance (MR) images were acquired using a 1.5-Tesla GE Neuro-optimised Signa MR system (General Electric, Milwaukee, WI, USA) fitted with 40 mT/m highspeed gradients, at the Maudsley Hospital, London. Foam padding and a forehead strap were used to limit head motion. A quadrature birdcage head coil was used for radio frequency (RF) transmission and reception. A total of 180 T2*-weighted MR brain volumes depicting blood-oxygen-level-dependent (BOLD) contrast were acquired at each of 36 near-axial, non-contiguous planes parallel to the inter-commissural (AC-PC) plane; repetition time (TR) = 3000ms, echo time (TE) = 40ms, slice thickness = 3mm, voxel dimensions = 3.75 x 3.75 x 3.30mm, matrix size = 64 * 64, flip angle=90°. Prior to each acquisition sequence, four dummy data acquisition scans were performed to allow the scanner to reach a steady state in T1 contrast.

During the same session, a high-resolution T1-weighted structural image was acquired in the axial plane (inversion recovery prepared, spoiled gradient-echo sequence; TR = 18ms, TE = 5.1 ms, TI = 450 ms, slice thickness = 1.5 mm, voxel dimensions = 0.9375 × 0.9375 x 1.5 mm, matrix size 256 * 192, field of view = 240 x 180 mm, flip angle = 20°, number of excitations = 1) for subsequent co-registration.

Image processing

All analyses were implemented using Statistical Parametric Mapping software, version 8 (SPM8) (www.fil.ion.ucl.ac.uk/spm/software/spm8/). The BOLD images were realigned to the fifth volume to correct for interscan movements by means of a rigid body

transformation with three rotation and three translation parameters. Subsequently, the 180 fMRI images were spatially normalized to the standard template of the Montreal Neurological Institute (MNI) and re-sampled to a voxel size of 2x2x2 mm. Finally, the images were smoothed using an 8 mm full width half maximum Gaussian kernel.

The smoothed single-participant images were analyzed via multiple regressions using the linear convolution model, with vectors of onset representing the experimental conditions (1, 2 and 3 - back) and the 0-back condition as a baseline. Six movement parameters were also entered as nuisance covariates. Serial correlations were removed using an AR(1) model. A high pass filter (128s) was applied to remove low-frequency noise. Contrast images of each memory load condition versus baseline were produced for each participant.

Conventional fMRI Analysis

Group-level analyses were based on random-effects analyses of the single-participant contrast images using the summary statistic approach. Regions showing significant task effect across all participants were identified using one-sample t-tests against zero. The statistical threshold was set to $p<0.05$ with Family-Wise Error (FWE) correction **on a voxelwise basis** and minimum cluster size 20 voxels. For all analyses, results are reported in MNI space.

Dynamic Causal Modeling

Selection of volumes of interest (VOIs)

Volumes of interest (VOIs) were defined bilaterally in the PAR, ACC and DLPFC based on evidence from prior studies demonstrating robust and consistent involvement of these regions in WM (Glahn et al., 2005; Owen et al., 2005) and based on the results from the

current analyses that found significant effects of WM load in these regions. The coordinates for the VOIs were based on the group maxima from the contrast of 1, 2, 3 -back minus 0-back condition following conjunction analysis. The coordinates of the group maxima were: DLPFC (left: x = -48, y = 36, z = 30; right; x = 48, y = 38, z = 30), PAR (left: x = -38, y = -56, z = 42; right: x = 36, y = -52, z = 44) and ACC (left: x = -10, y = 26, z = 28; right: x = 12, y =24, z =28) and the). For each participant VOIs of 5mm radius were defined centred on participant-specific maxima in these regions that were (i) within 4 mm from the group maxima, (ii) within the same anatomical area, as defined by the PickAtlas toolbox (Maldjian et al., 2003) and (iii) adjusted using the effect of interest F-contrast. Regional time series were summarised with the first eigenvariate of all activated (at $p < 0.01$) voxels within the participant-specific VOIs.

Specification of model architecture

For each experimental condition (1, 2, 3 –back) we used the VOIs defined above (L-PAR and R-PAR, L-ACC and R-ACC, and L-DLPFC and R-DLPFC) to specify a six-area DCM in all participants. Within each hemisphere we defined bidirectional connections between these regions. Bidirectional connections were also specified between homologous regions in each hemisphere. For each experimental condition, 18 endogenous connections were specified in total with the main effect of memory as the driving input entering the L-PAR and R-PAR (Figure 1A). This architecture served as our base model which was then elaborated systematically to produce 18 alternative variants for each experimental condition **to test how working memory load could modulate the 18 connections** (Figure 1B). In total 54 models were constructed, fitted and compared in the 40 study participants.

Model Comparison

Model comparison was implemented using random-effects (RFX) Bayesian Model Selection (BMS) in DCM10 to compute exceedance and posterior probabilities at the group level (Stephan et al., 2009). The exceedance probability of a model denotes the probability that this model is more likely than any other in a given dataset. In addition to testing individual models we also made inferences about Families of models (Penny et al., 2010; Stephan et al., 2010).

Families were specified based on laterality and direction of **working memory information**. To test for hemispheric laterality, models were divided into a Left-sided (Models 1, 3, 4, 5, 6, 7, 9, 10, 11) and a Right-sided Family (Models 2, 8, 12, 13, 14, 15, 16, 17, 18). To test for directionality of **working memory information** three Families where created for each experimental condition, Forward (Models 3, 5, 10, 14, 16, 17), Backwards (Models 4, 6, 9, 13, 15, 18) and Lateral (Models 1, 2, 7, 8, 11, 12). All models were included in the BMS procedure, both when comparing individual models and model Families. Finally, to summarise the strength of effective connectivity and quantify its modulation, we used random effects Bayesian Model Averaging (BMA) to obtain average connectivity estimates (weighted by their posterior model probability) across all models for each participant (Penny et al., 2010). The implementation of RFX BMA in SPM8 employs an Occam's window for computational efficiency, excluding from the average those models whose probability ratio (compared to the best model) is below 0.05.

Relationship to behavioural measures

We subjected participant-specific BMA parameter estimates to one-sample tests to assess their consistency across participants. Behavioural data and DCM parameter estimates were analyzed in SPSS 20 (SPSS Inc, Chicago, IL, USA) and statistical inference was set at a threshold of $p<0.002$ following Bonferroni-correction for multiple comparisons.

Results

Behavioural data

Details of participants' performance in the n-back task are shown in Table 1.

Conventional fMRI analysis

Task-related activation was evident within the predicted WM network including the DLPFC, PAR and ACC. Details of the regional maxima are provided in Figure 2 and Table 2.

DCM analysis

Family-wise Comparisons

We applied random effects BMS at the Family level to clarify the contribution of each hemisphere (Left: Models 1, 3, 4, 5, 6, 7, 9, 10, 11; Right: Models 2, 8, 12, 13, 14, 15, 16, 17, 18) and to elucidate the direction of information (Forward, Backward or Lateral) at different memory loads. The Left-sided Family showed the highest exceedance probability (65%; Figure 3A) in the 1-back modulation. This pattern reversed in the 2- and 3-back modulations where the Right-sided Family showed exceedance probabilities of 60% and 98% respectively (Figures 3B and 3C).

With regards to directionality, in the 1-back modulation the Forward Family showed an exceedance probability of 52% followed by the Backward Family with an exceedance

probability of 32% (Figure 3A). In the 2- and 3-back modulations, the Forward Family outperformed all others with an exceedance probability of 99% (Figure 3B and 3C).

Comparing individuals models

Comparing the individuals models in each memory load, did not reveal an optimal model for the 1-back modulation (Figure 4A). On the contrary, for the 2-back memory load, Model 16 was the best fitting model with exceedance probability of 60%, where the modulation was placed from the R-PAR to the R-DLPFC (Figure 4B). Model 5 was the second best model with exceedance probability of 40%. In Model 5, 2-back modulated the forward connection from L-PAR to L-DLPFC (Figure 4B).

For the 3-back task, Model 16 outperformed all other models with an exceedance probability of 96%, where the 3-back memory load is modulating significantly the forward connection from the R-PAR to the R-DLPFC (Figure 4C).

Bayesian Model Averaging

The results from the BMA across all subjects and across all fifty four models (18 models for each experimental condition) are shown in Table 3. All connections between the six areas of the WM network were significant. BMA parameter estimates of the endogenous connections were found to be significantly consistent across participants. The task condition significantly modulated the forward connection from the R-PAR to the R-DLPFC (Table 3).

Behavioural Correlations

Based on the robust modulation of the connection from the R-PAR to the R-DLPFC by increasing memory load we performed correlations between the DCM parameters for this connection in the 3-back condition with response time and accuracy. The WM modulation

of this connection negatively correlated with response time (r= -0.331, p= 0.04) but not accuracy in the 3-back condition.

Discussion

To our knowledge this is the first study to assess effective connectivity during WM processing using DCM. DCM is currently one of the most plausible methods for inferring neuroplastic changes in the strength of connections between neuronal populations and their context specific (Stephan et al., 2010). There are three key findings from our study. First, we demonstrated that increasing memory load was associated with increasing dominance of right-hemisphere models suggesting greater right hemisphere contribution to the most demanding WM conditions. Second, increasing memory load was associated with increased forward (i.e. posterior to anterior) effective connectivity within the WM network. Third, increasing memory load dramatically reduced individual variability in WM network architecture with the right-hemisphere forward model reaching an exceedance probability of 99% in the 3-back condition.

Early fMRI studies have lent support to the notion that processing within the WM network is left-lateralised for verbal and right-lateralised for spatial material (Fletcher and Henson, 2001). Recent quantitative meta-analyses have shown that engagement during verbal WM tasks can be seen bilaterally within the DLPFC, PAR and ACC (Wager and Smith, 2003; Nee et al., 2013) although left-sided involvement was more common (Nee et al., 2013). However previous studies (Altamura et al., 2007; Kirschen et al., 2005) as well as the current study suggest that the key driver of lateralisation within the verbal WM network is memory load. In the 1-back condition the Left-sided model Family showed an aggregate exceedance probability of 65% while in the 2-back condition the Right-sided model Family

showed an aggregate exceedance probability of 60%. These exceedance probabilities are moderate and may be best interpreted as evidence that right or left hemispheric involvement is nearly equally plausible at low to moderate WM demands. By contrast, in the 3-back condition, that places the highest demands on maintenance and updating processes, the Right-sided model Family was dominant with an exceedance probability of 98%.

Previous literature has established that during a variety of WM tasks ipsilateral frontoparietal cortical regions are functionally coupled (Esslinger et al., 2012; Cole and Schneider, 2007; Schlosser et al., 2006). The current study provides new evidence regarding the directionality of effective coupling within the verbal WM network. We found that **working memory information** follows a posterior to anterior direction at moderate and high WM load as the Forward model Family showed an exceedance probability of 99% in the 2- and 3-back conditions. In particular the connection from the right PAR to the ipsilateral DLPFC was most consistently modulated by WM across all participants; the strength of the modulation increased with WM demands and was associated with reduced response time. Our findings receive significant support from transcranial magnetic stimulation (TMS) studies (Mottaghy et al., 2003; Esslinger et al., 2012; Meiron et al., 2012); TMS induced increase in frontoparietal coupling improved response time without a significant effect on accuracy. Correspondingly we observed a significant correlation between response time (but not accuracy) and the strength of the WM modulation of the frontoparietal effective connectivity. Mottaghy and colleagues (2003) were also able to determine using TMS at variable time points and at different cortical sites that during the verbal n-back task information propagated from posterior to anterior regions (parietal to prefrontal) and from the right to the left prefrontal cortex. This observation is consistent with our findings regarding the dominance of the forward right hemisphere model Families and the

importance of the connection between right PAR and right DLPFC. Moreover, our data further support the proposal of Mottaghy and colleagues (2003) that verbal WM performance may rely on successful coding of the visual input of letters first as objects in the right hemisphere and then as verbal concepts in the left hemisphere.

A feature of our experimental design merits comment. We employed the n-back task as a fMRI block paradigm, which precludes the possibility of including only trials on which participants answered correctly in our analysis. Considering the difference in accuracy and reaction time between memory loads, as would be expected, future studies investigating the effect of working memory may wish to employ tasks that permits that kind of analysis. Furthermore, the DCM models in the current study were constructed to probe cognitive control in the WM brain network. Future studies may also wish to include brain areas typically engaged in verbal WM, such as left perisylvian regions (Rottschy et al., 2012), to investigate the verbal WM network directly.

Finally we found that increasing WM load dramatically reduced variability in the dynamic architecture of the WM network. The interest in **short-term plasticity** has generated much research on the effect of task on neural variability at all levels. Task-related reduction in variability has been observed throughout the cortex at the intracellular and inter-cellular level affecting membrane potential as well as individual and correlated neuronal firing (Churchland et al., 2010). Theoretical models have suggested similar properties for large scale neural networks (Sussillo & Abbott, 2009; Rajan et al. 2012). Our results provide direct empirical support for these models with regards to WM and further suggest that task difficulty is a significant additional moderator of **short-term plasticity**.

Acknowledgements: This work was supported by a NARSAD Independent Investigator Award 2008 (S.F.).

References

Altamura M, Elvevag B, Blasi G, Bertolino A, Callicott JH, Weinberger DR, Mattay VS, Goldberg TE (2007): Dissociating the effects of Sternberg working memory demands in prefrontal cortex. Psychiatry Research: Neuroimaging 154:103-114.

Axmacher N, Schmitz DP, Wagner T, Elger CE, Fell J (2008): Interactions between medial temporal lobe, prefrontal cortex and inferior temporal regions during visual working memory: A combined intracranial EEG and functional magnetic resonance imaging study. J Neurosci 28:7304-7312.

Baddeley A (1992): Working Memory: The Interface between Memory and Cognition. J Cogn Neurosci 4:281–288.

Braver TS, Cohen JD, Nystrom LE, Jonides J, Smith EE, Noll DC (1997): A parametric study of prefrontal cortex involvement in human working memory. Neuroimage 5:49-62.

Callicott JH, Mattay VS, Bertolino A, Finn K, Coppola R, Frank JA, Goldberg TE, Weinberger DR (1999): Physiological characteristics of capacity constraints in working memory as revealed by functional MRI. Cereb Cortex 9:20-26.

Carter CS, Botvinick MM, Cohen JD (1999): The contribution of the anterior cingulate cortex to executive processes in cognition. Rev Neurosci 10:49-57.

Churchland MM, Yu BM, Cunningham JP, Sugrue LP, Cohen MR, Corrado GS, Newsome WT, Clark AM, Hosseini P, Scott BB, Bradley DC, Smith MA, Kohn A, Movshon JA, Armstrong KM, Moore T, Chang SW, Snyder LH, Lisberger SG, Priebe NJ, Finn IM, Ferster D, Ryu SI, Santhanam G, Sahani M, Shenoy KV (2010): Stimulus onset quenches neural variability: a widespread cortical phenomenon. Nat Neurosci 13:369-78.

Cole MW, Schneider W (2007): The cognitive control network: Integrated cortical regions with dissociable functions. Neuroimage 37:343–360.

Cramer SC, Sur M, Dobkin BH, O'Brien C, Sanger TD, Trojanowski JQ, Rumsey JM, Hicks R, Cameron J, Chen D, Chen WG, Cohen LG, deCharms C, Duffy CJ, Eden GF, Fetz EE, Filart R, Freund M, Grant SJ, Haber S, Kalivas PW, Kolb B, Kramer AF, Lynch M, Mayberg HS, McQuillen PS, Nitkin R, Pascual-Leone A, Reuter-Lorenz P, Schiff N, Sharma A, Shekim L, Stryker M, Sullivan EV, Vinogradov S (2011): Harnessing neuroplasticity for clinical applications. Brain 134:1591–1609.

D'Esposito M, Postle BR, Rypma B (2000): Prefrontal cortical contributions to working memory: Evidence from event-related fMRI studies. Exp Brain Res 133:3–11.

Esslinger C, Schüler N, Sauer C, Gass D, Mier D, Braun U, Ochs E, Schulze TG, Rietchel M, Kirsch P, Meyer-Lindenberg A (2012): Induction and quantification of prefrontal cortical network plasticity using 5Hz rTMS and fMRI. Hum Brain Mapp (in press) doi: 10.1002/hbm.22165

First MB, Spitzer RL, Gibbon M, Williams JBW. 2002. Structured Clinical Interview for DSM-IV Axis I Disorders, Research Version, Non-patient Edition (SCID-I/NP). New York, NY: Biometrics Research, New York State Psychiatric Institute.

Fletcher PC, Henson RN (2001): Frontal lobes and human memory: Insights from functional neuroimaging. Brain 124: 849–881.

Friston KJ, Harrison L, Penny WD (2003): Dynamic Causal Modeling. Neuroimage 19:1273-1302.

Glahn DC, Ragland JD, Abramoff A, Barrett J, Laird AR, Bearden CE, Velligan DI (2005): Beyond hypofrontality: a quantitative meta-analysis of functional neuroimaging studies of working memory in schizophrenia. Hum Brain Mapp 25:60-69.

Guerin SA, Miller MB (2011): Parietal cortex tracks the amount of information retrieved even when it is not the basis of a memory decision. Neuroimage 55: 801-807.

Honey GD, Fu CH, Kim J, Brammer MJ, Croudace TJ, Suckling J, Pich EM, Williams SC, Bullmore ET (2002): Effects of verbal working memory load on corticocortical connectivity modeled by path analysis of functional magnetic resonance imaging data. Neuroimage 17:573-582.

Jonides J, Schumacher EH, Smith EE, Koeppe RA, Awh E, Reuter-Lorenz PA, Marshuetz C, Willis CR (1998): The role of parietal cortex in verbal working memory. J Neurosci 18:5026 –5034.

Kim JS, Jung WH, Kang DH, Park JY, Jang JH, Choi JS, Choi JH, Kim J, Kwon JS (2012): Changes in Effective Connectivity According to Working Memory Load: An fMRI Study of Face and Location Working Memory Tasks. Psychiatry Investig 9:283-292.

Kim J, Zhu W, Chang L, Bentler PM, Ernst T (2007): Unified Structural Equation Modeling Approach for the Analysis of Multisubject, Multivariate Functional MRI Data. Hum Brain Map 28:85-93.

Kirschen MP, Chen ASH, Schraedley-Desmond P, Desmond JE (2005): Load- and practice-dependent increases in cerebro-cerebellar activation in verbal working memory: an fMRI study. NeuroImage 24:462-472.

Maldjian JA, Laurienti PJ, Kraft RA, Burdette JH (2003): An automated method for neuroanatomic and cytoarchitectonic atlas-based interrogation of fMRI data sets. Neuroimage 19:1233-1239.

Meiron O, Lavidor M (2013): Unilateral prefrontal direct current stimulation effects are modulated by working memory load and gender. Brain Stimul 6:440-447.

Mottaghy FM, Gangitano M, Krause BJ, Pascual-Leone A (2003): Chronometry of parietal and prefrontal activations in verbal working memory revealed by transcranial magnetic stimulation. Neuroimage 18:565-575.

Narayanan NS, Prabhakaran V, Bunge SA, Christoff K, Fine EM, Gabrieli JDE (2005): The role of the prefrontal cortex in the maintenance of verbal working memory: an event-related fMRI analysis. Neuropsychology 19:223-232.

Nee DE, Brown JW, Askren MK, Berman MG, Demiralp E, Krawitz A, Jonides J (2013): A meta-analysis of executive components of working memory. Cereb Cortex 23:264-282.

Owen AM, Herrod NJ, Menon DK, Clark JC, Downey SPMJ, Carpenter TA, Minhas PS, Turkheimer FE, Williams EJ, Robbins TW, Sahakian BJ, Petrides M, Pickard JD (1999): Redefining the functional organization of working memory processes within human lateral prefrontal cortex. Eur J Neurosci 11:567-574.

Owen AM, McMillan KM, Laird AR, Bullmore ET (2005): N-back working memory paradigm: a meta-analysis of normative functional neuroimaging studies. Hum Brain Mapp 25:46-59.

Paulesu E, Frith CD, Frackowiak, RS (1993): The neural correlates of the verbal component of working memory. Nature 362:342–345.

Penny WD, Stephan KE, Daunizeau J, Rosa MJ, Friston KJ, Schofield TM, Leff AP (2010): Comparing Families of Dynamic Causal Models. PLoS Comput Biol 6:1-14.

Rajan K, Abbott LF, Sompolinsky H (2010): Stimulus-dependent suppression of chaos in recurrent neural networks. Phys Rev E Stat Nonlin Soft Matter Phys 82:011903.

Ramnani N, Behrens T, Penny WD, Matthews PM (2004): New approaches for exploring anatomical and functional connectivity in the human brain. Biol Psychiatry 56:613–619.

Rottschy C, Langner R, Dogan I, Reetz K, Laird AR, Schulz JB, Fox PT, Eickhoff SB (2012): Modelling neural correlates of working memory: a coordinate-based meta-analysis. Neuroimage 60:830-846.

Salinas E, Sejnowski TJ (2001): Gain modulation in the central nervous system: where behavior, neurophysiology, and computation meet. Neuroscientist 7:430-440.

Sala-Llonch R, Peña-Gómez C, Arenaza-Urquijo EM, Vidal-Piñeiro D, Bargalló N, Junque Carme, Bartres-Faz D (2012): Brain connectivity during resting state and subsequent working memory task predicts behavioural performance. Cortex 48:1187-1196.

Schlosser RG, Wagner G, Sauer H (2006): Assessing the working memory network: Studies with functional magnetic resonance imaging and structural equation modeling. Neuroscience 139:91–103.

Stephan KE, Baldeweg T, Friston KJ (2006): Synaptic plasticity and dysconnection in schizophrenia. Biol Psychiatry 59:929-939.

Stephan KE, Penny WD, Daunizeau J, Moran RJ, Friston KJ (2009): Bayesian model selection for group studies. Neuroimage 15:1004-1017.

Stephan KE, Penny WD, Moran RJ, den Ouden HEM, Daunizeau J, Friston KJ (2010): Ten simple rules for dynamic causal modeling. Neuroimage 49:3099-3109.

Sussillo D, Abbott LF (2009): Generating coherent patterns of activity from chaotic neural networks. Neuron 63:544-557.

Volle E, Kinkingnéhun S, Pochon JB, Mondon K, Thiebaut de Schotten M, Seassau M, Duffau H, Samson Y, Dubois B, Levy R (2008): The functional architecture of the left posterior and lateral prefrontal cortex in humans. Cereb Cortex 18:2460-2469.

Wager TD, Smith EE (2003): Neuroimaging studies of working memory: a meta-analysis. Cogn Affect Behav Neurosci 3:255-274.

Wechsler D. 1981. Manual for the Wechsler Adult Intelligence Scale—Revised. New York, NY: Psychological Corporation.

Figure Legends

Figure 1. Model specification: The sources comprising the models were: DLPFC: dorsolateral prefrontal cortex; PAR: parietal; ACC: dorsal anterior cingulate cortex; left and right. Schematically, the modulations are represented as one memory load (•), but correspond to the three distinct modulations: 1-back, 2-back and 3-back. **A.** A six-area DCM was specified with bidirectional endogenous connections between all regions (PAR, ACC, DLPFC) in each hemisphere and lateral connections between homologous areas. Driving input of '1, 2, 3 -back' modelled into the left and right PAR. **B.** For each memory load (1, 2, 3 -back condition) 18 models were constructed.

Figure 2. A. Image showing task-related brain activation in the group (N=40) during the working memory N-back task (FWE, corrected at $p<0.05$ **on a voxelwise basis**, minimum cluster size 20 voxels; image created with MRIcron http://www.mccauslandcenter.sc.edu/mricro/mricron/index.html). **B.** The effect of the 1, 2, 3 -back conditions on the left and right parietal cortex (PAR), the left and right anterior cingulate cortex (ACC), left and right dorsolateral prefrontal cortex (DLPFC) in healthy participants (N=40).

Figure 3. A. Family Exceedance Probability for the Left- and Right-sided Family, as well as the Forward, Backward and Lateral Family in the 1-back condition (N=40). **B.** Family Exceedance Probability for the Left and Right-sided Family, as well as the Forward, Backward and Lateral Family in the 2-back condition (N=40). **C.** Family Exceedance

Probability for the Left and Right-sided Family, as well as the Forward, Backward and Lateral Family in the 3-back condition (N=40).

Figure 4A. Exceedance Probability for the eighteen models specified (N=40) in the 1-back condition. Yellow lines represent the Models that have Exceedance Probability above 5%. **B.** Exceedance Probability for the eighteen models specified (N=40) in the 2-back condition. Yellow lines represent the two winning models, Model 5 and Model 16. **C.** Exceedance Probability for the eighteen models specified (N=40) in the 3-back condition. Yellow line represents the optimal Model 16.

Table 1. Demographic and behavioural data of study participants (n=40)

Demographic data	
Sex (male:female)	20:20
Age (years)	31.5 (10.4)
WAIS-R IQ	115.5 (15.9)
Behavioural Performance on the n-back task	
Response time, 1-back (ms)	596 (210)
Accuracy, 1-back (% correct)	100
Response time, 2-back (ms)	659 (196)
Accuracy, 2-back (% correct)	91.2 (13.85)
Response time, 3-back (ms)	748 (224)
Accuracy, 3-back (% correct)	72.8 (16.1)

Continuous variables are presented as mean and standard deviation;
WAIS-R=Wechsler Adult Intelligence Scale-Revised

Table 2. Voxel-based whole brain SPM analysis: Brain regions showing significant main effects in terms of hemodynamic responses to different working memory loads; 1, 2, 3 -back ($p < 0.05$, FWE cluster-level corrected across the whole brain with minimum cluster size 20 voxels).

Brain Region	**BA**	**Laterality**	**Coordinates**			**Cluster Size (voxels)**	**Z - value**
			x	**y**	**z**		
1-back > 0-back							
Inferior parietal lobule	40	R	46	-46	44	121	6.61
	40	L	-44	-42	38	754	6.31
Middle frontal gyrus	46	L	-46	32	30	153	6.42
(Dorsolateral PFC)		R	52	36	30	256	6.30
Middle frontal gyrus	6	R	32	6	62	47	5.97
2-back > 0-back							
Inferior parietal lobule	40	R	40	-48	44	231	7.90
		L	-36	-52	46	190	7.75
Middle frontal gyrus	46	R	46	32	28	544	7.03
(Dorsolateral PFC)	9	L	-42	8	28	968	6.64
Anterior cingulate gyrus	32	R	8	18	48	354	6.88
		L	-4	10	58		
Insula	13	R	34	24	-2	151	6.47
Middle frontal gyrus	6	R	30	8	58	414	6.12

3-back > 0-back							
Inferior parietal lobule	40	R	50	-42	42	287	8.01
		L	-48	-48	48	263	7.98
Middle frontal gyrus	9	L	-48	26	30	800	8
(Dorsolateral PFC)	46	R	48	40	30	542	7.99
Anterior cingulate gyrus	32	L	-10	26	30	333	7.53
		R	8	20	28		
Insula	13	L	-34	22	0	680	6.99
Thalamus	N/A	L	-12	-10	6	142	6.44
Inferior frontal gyrus	10	L	-44	46	2	319	5.98
Inferior frontal gyrus	47	R	34	20	0	572	5.67

MNI coordinates denote the distance in mm from the anterior commissure, with positive X= right of midline, positive Y = anterior to the anterior commissure, and positive Z = dorsal to a plane containing both the anterior and the posterior commissures. Abbreviations: BA: Brodmann Area; ; L: Left; R: Right; N/A: Not Applicable; PFC: prefrontal cortex; SPM=Statistical Parametric Mapping.

Table 3. Dynamic Causal Modeling endogenous parameter and modulatory estimates for all connections across all subjects and across all models.

Connection type	**Mean**	**SD**	**Minimum**	**Maximum**	**T-value**	**P- value**
Endogenous parameters						
L-PAR→R-PAR	0.012	0.322	-1.876	1.007	2.727¥	0.000**
R-PAR→L-PAR	0.008	0.162	-1.049	0.120	2.639¥	0.000**
L-PAR→L-ACC	0.091	0.086	-0.159	0.266	7.154	0.000**
L-ACC→L-PAR	0.006	0.012	-0.024	0.047	3.294	0.002**
L-PAR→L-DLPFC	0.239	0.150	-0.039	0.654	10.818	0.000**
L-DLPFC→L-PAR	0.017	0.050	-0.049	0.305	2.413	0.020*
L-ACC→R-ACC	0.017	0.023	-0.005	0.090	5.106	0.000**
R-ACC→L-ACC	0.020	0.034	-0.001	0.150	4.119	0.000**
L-DLPFC→L-ACC	0.028	0.033	-0.015	0.095	5.910	0.000**
L-ACC→L-DLPFC	0.021	0.047	-0.218	0.127	3.115	0.003*
L-DLPFC→R-DLPFC	0.099	0.086	-0.025	0.304	7.809	0.000**
R-DLPFC→L-DLPFC	0.119	0.100	-0.025	0.304	8.003	0.000**
R-DLPFC→R-ACC	0.047	0.049	-0.071	0.158	6.519	0.000**
R-ACC→R-DLPFC	0.039	0.042	-0.022	0.157	6.384	0.000**
R-DLPFC→R-PAR	0.043	0.109	-0.082	0.685	1.936¥	0.001**
R-PAR→R-DLPFC	0.281	0.147	-0.111	0.493	12.982	0.000**
R-PAR→R-ACC	0.098	0.084	-0.048	0.282	7.930	0.000**
R-ACC→R-PAR	0.006	0.023	-0.085	0.086	1.948	0.05

Connection type	**Mean**	**SD**	**Minimum**	**Maximum**	**T-value**	**P- value**
Modulatory parameters in 3-*back*						
R-PAR→R-DLPFC	0.102	0.073	-0.039	0.292	9.431	0.000**

* p<0.05 uncorrected for multiple comparisons; ** p<0.002 corrected for multiple comparisons; ¥ Mann–Whitney U test; SD=standard deviation

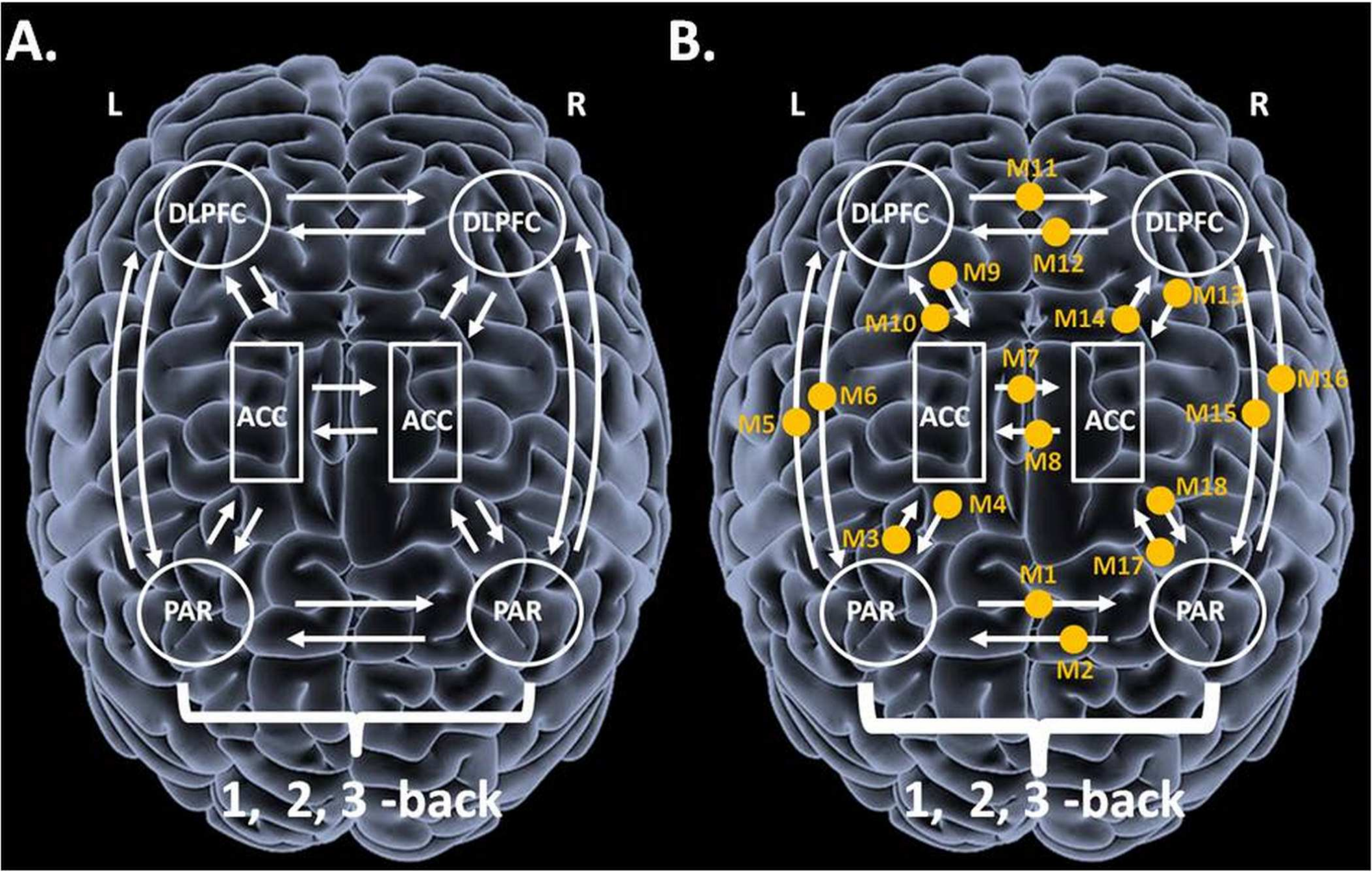
A.
L
R
DLPFC
DLPFC
ACC
ACC
PAR
PAR
1, 2, 3 -back
B.
L
R
M11
DLPFC
DLPFC
M12
M9
M13
M10
M14
M7
M16
M6
M5
ACC
ACC
M15
M8
M18
M4
M3
M17
M1
PAR
PAR
M2
1, 2, 3 -back

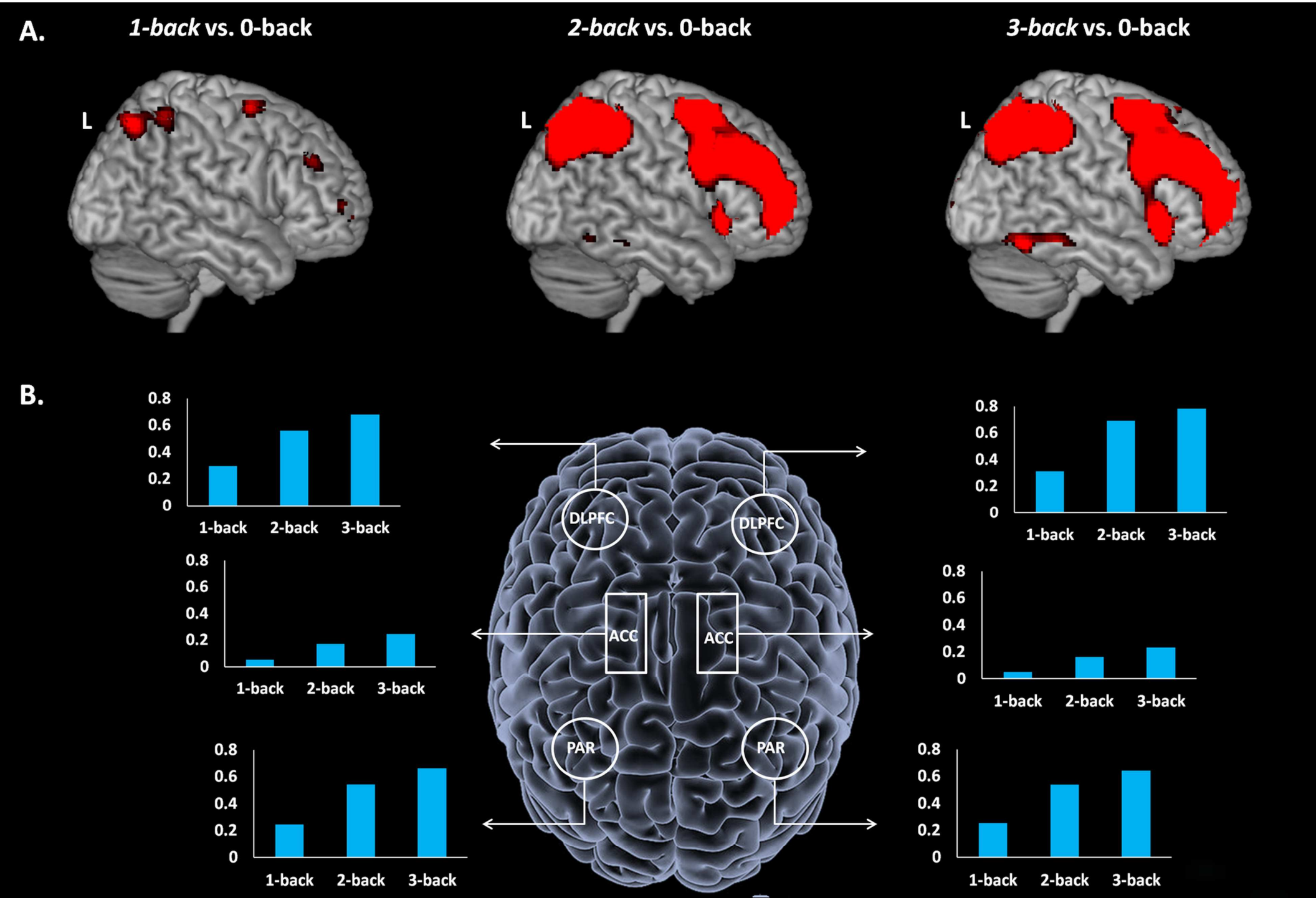
A.
1-back vs. 0-back
2-back vs. 0-back
3-back vs. 0-back
L
L
L
B.
0.8
0.6
0.4
0.2
0
1-back
2-back
3-back
DLPFC
DLPFC
ACC
ACC
PAR
PAR

A. 1-back

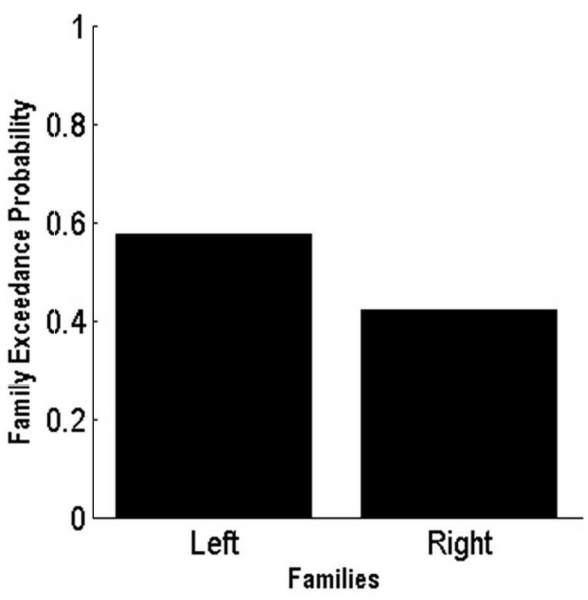

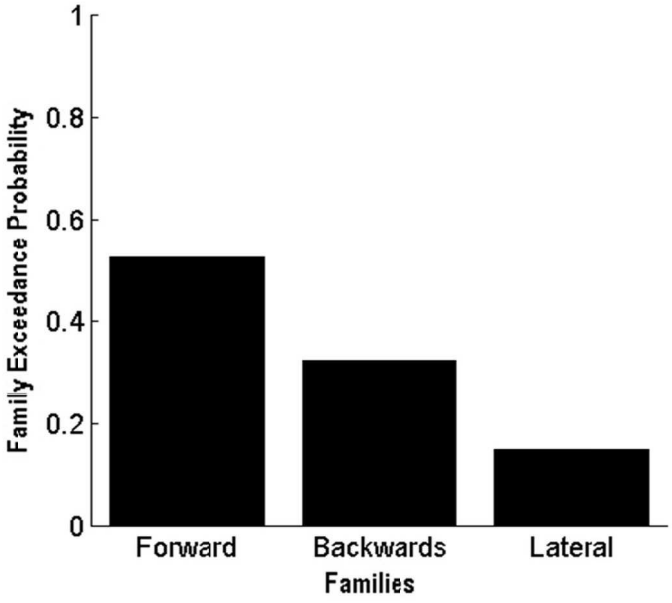

B. 2-back

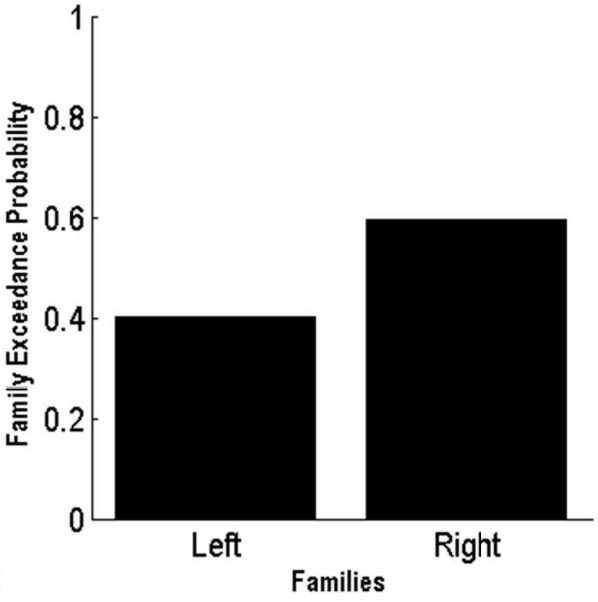

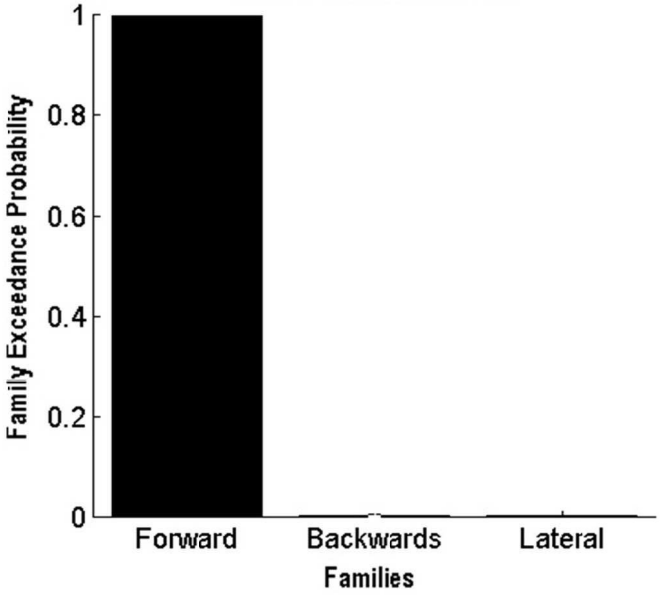

C. 3-back

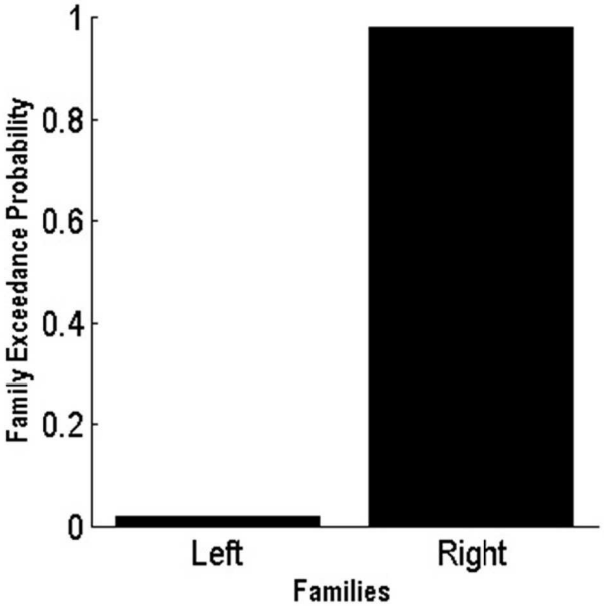

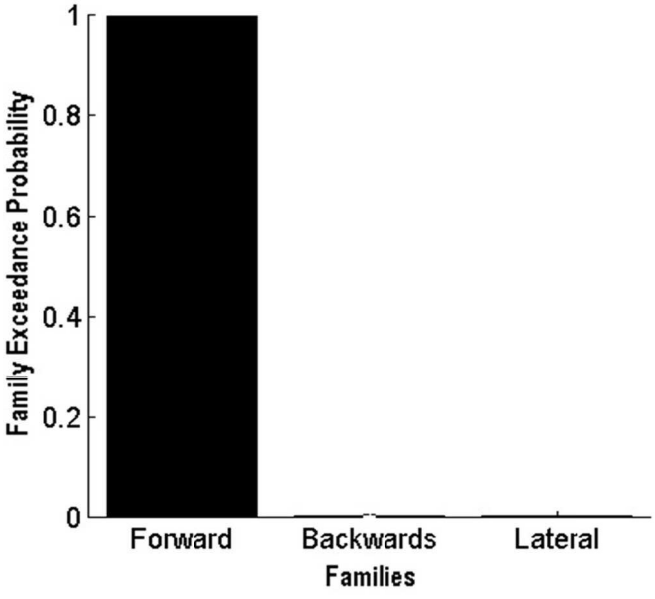

A. 1-back

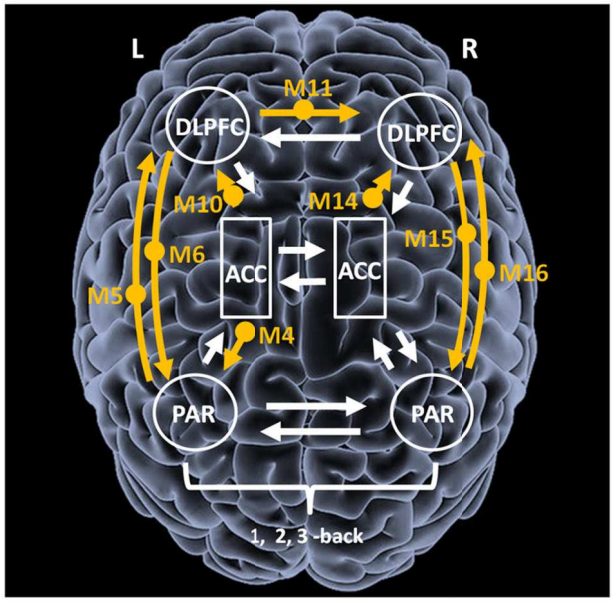

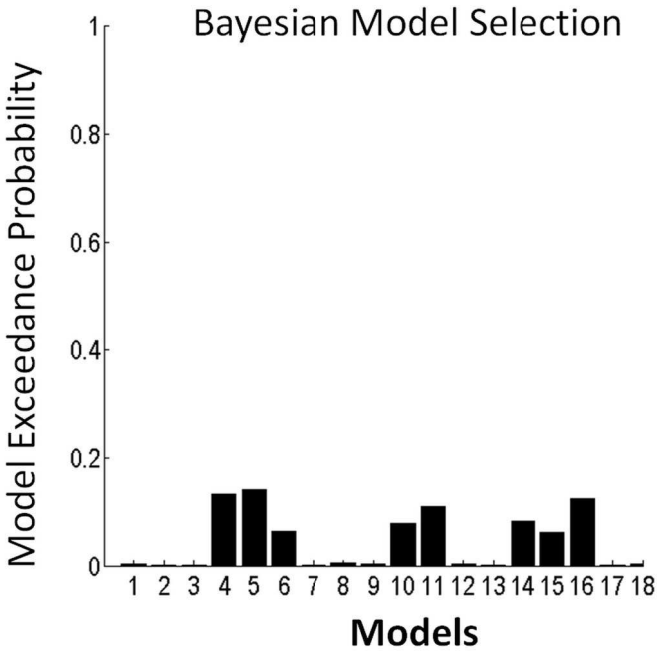

B. 2-back

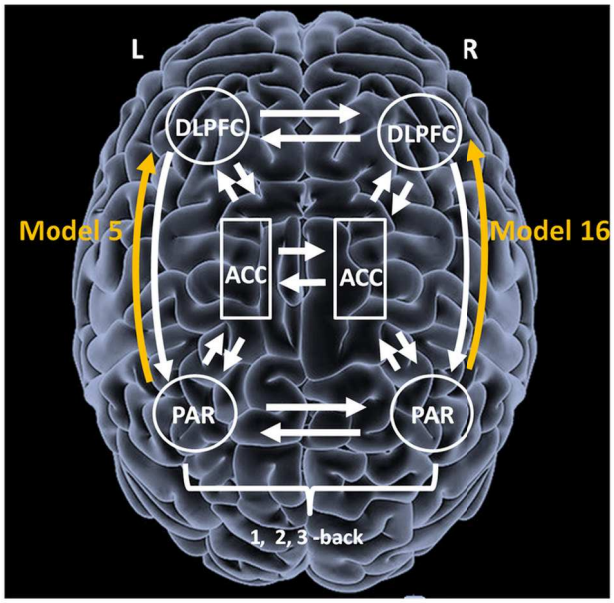

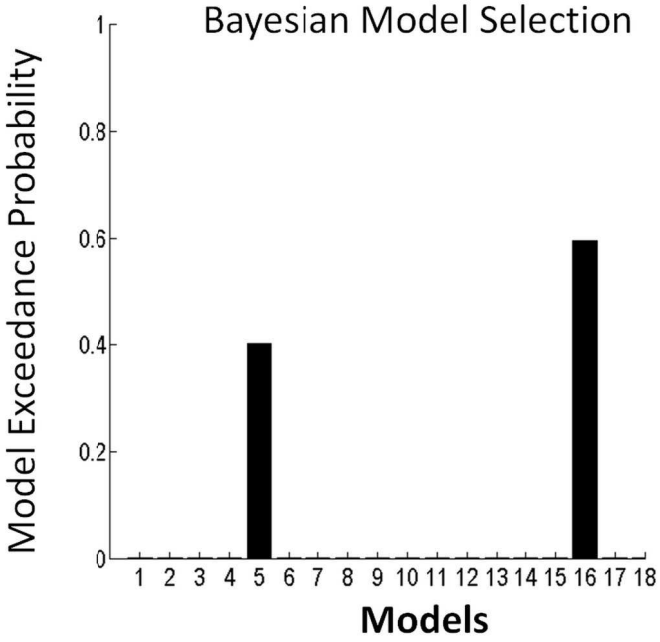

C. 3-back

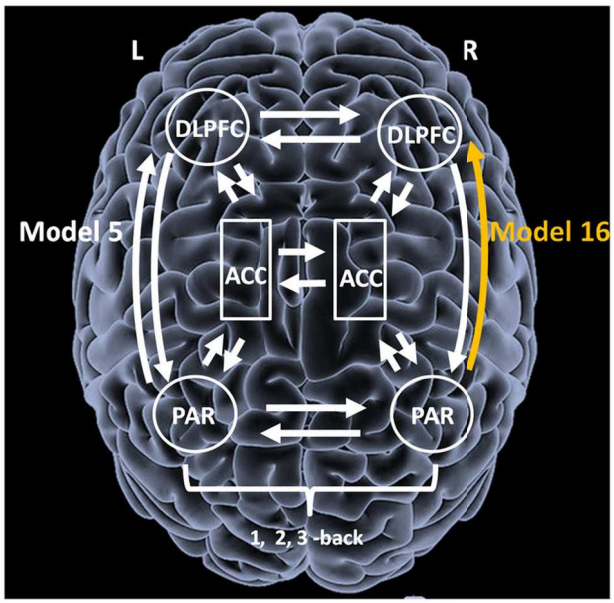

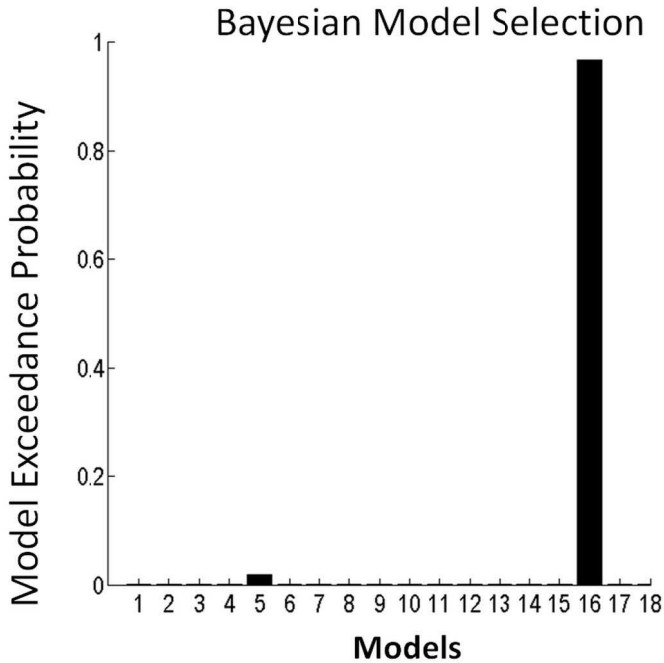

Legend for Supplemental Figure 1.

The sources comprising the models were: DLPFC: dorsolateral prefrontal cortex; PAR: parietal; ACC: dorsal anterior cingulate cortex; left and right. A six-area DCM was specified with bidirectional endogenous connections between all regions (PAR, ACC, DLPFC) in each hemisphere and lateral connections between homologous areas. Driving input of '1, 2, 3 -back' modelled into the left and right PAR. Schematically, the modulations are represented as one memory load (•), but correspond to the three distinct modulations: 1-back, 2-back and 3-back. For each memory load (1, 2, 3 -back condition) 18 models were constructed.

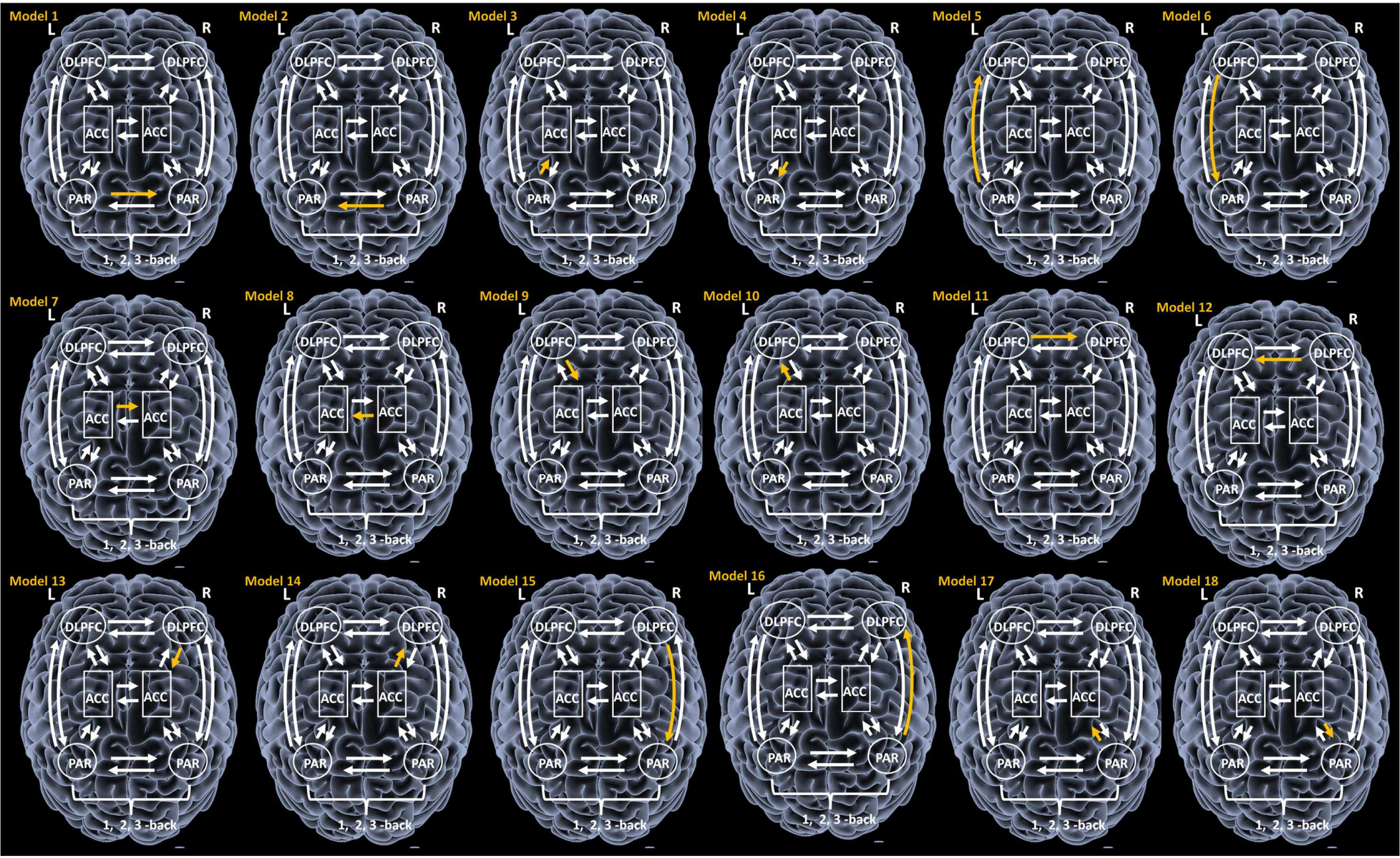
Model 1
Model 2
Model 3
Model 4
Model 5
Model 6
Model 7
Model 8
Model 9
Model 10
Model 11
Model 12
Model 13
Model 14
Model 15
Model 16
Model 17
Model 18
L
R
DLPFC
ACC
PAR
1, 2, 3 -back